Adiabatic creation of entangled states by a bichromatic field designed from the topology of the dressed eigenenergies

S. Guérin,[1,*] R. G. Unanyan,[2,3] L. P. Yatsenko,[4,†] and H. R. Jauslin[1]

[1]*Laboratoire de Physique, UMR CNRS 5027, Université de Bourgogne, Boîte Postale 47870, 21078 Dijon, France*

[2]*Fachbereich Physik, Universitität Kaiserslautern, 67653 Kaiserslautern,Germany*

[3]*Institute for Physical Research, Armenian National Academy of Sciences, 378410 Ashtarak, Armenia*

[4]*Institute of Physics of the Ukrainian Academy of Sciences, prospekt Nauky, 46, 252650 Kiev-22, Ukraine*

(Received 28 February 2002; published 18 September 2002)

Preparation of entangled pairs of coupled two-state systems driven by a bichromatic external field is studied. We use a system of two coupled spin-$\frac{1}{2}$ particles that can be translated into a three-state ladder model whose intermediate state represents the entangled state. We show that this entangled state can be prepared in a robust way with appropriate fields. Their frequencies and envelopes are derived from the topological properties of the model.

DOI: 10.1103/PhysRevA.66.032311 PACS number(s): 03.67.−a, 42.50.Hz, 03.65.Ta

I. INTRODUCTION

Entanglement is a key concept in various contemporary areas of active research in quantum physics. It explicitly demonstrates the nonlocal character of quantum theory, having potential applications in quantum communication, cryptography, and computation [1]. The preparation of an entangled state is of great interest for both fundamental and applied reasons. During the last few years various methods for preparation of entangled states of atomic systems have been proposed and some of them experimentally demonstrated [2,3].

Although a quantum system can be manipulated by tailored sequences of resonant pulses of precise area, in particular, π and $\pi/2$ pulses, respectively, for the complete inversion and the equal weight coherent superposition, deviations from the precise pulse area and from resonance can lead to significant errors. Adiabatic passage techniques provide much greater robustness against fluctuations in the interaction parameters. The stimulated Raman adiabatic passage (STIRAP) method [4] has been proposed for the creation of an entangled state of two three-level atoms in a QED cavity [5] and for Λ atomic systems [6].

In this paper we propose a simple method for entangling two subsystems driven by pulse-shaped external fields. For definiteness, we take these to be two identical spins interacting with each other and driven by radio-frequency fields. This system can be translated in a three-level ladder model with the intermediate level corresponding to the entangled state [7]. The goal is to populate completely this entangled state at the end of the pulses by adiabatic passage. The most efficient couplings are obtained with two near one-photon resonant fields. We will show that unlike in the STIRAP process, one- and two-photon detunings are required to populate most efficiently the intermediate level.

We show furthermore that bichromatic effects play an important role, due to the small anharmonicity of the system. The anharmonicity of the equivalent three-level ladder system is determined by the interaction of the spins. It can be in general small enough such that the standard rotating wave approximation (RWA), allowing to assign each field to a unique transition, cannot be applied. In this case one needs to take full account of the bichromatic effects (see, e.g., Ref. [8]). We will show robust regions of field parameters that will generate the entangled state by adiabatic passage below and beyond the standard RWA.

In Sec. II, we describe the model of the two-spin system driven by a bichromatic external field and how it leads to an equivalent three-level system. In Sec. III, we show the result of numerical simulations, for which we develop in later sections a detailed interpretation by constructing adapted effective Hamiltonians that take into account the dominating resonant or quasiresonant effects. In Sec. IV, we derive the Floquet Hamiltonian required to study the system of spins dressed by the external fields. Sections V and VI are devoted to derive relevant effective dressed Hamiltonians for different regions of parameters, respectively, in the weak field regime (below the RWA) and in the strong field regime (beyond the RWA). We finally conclude in Sec. VII.

II. THE MODEL: TWO-SPIN SYSTEM IN EXTERNAL FIELDS

We consider two-spin-$\frac{1}{2}$ particles of the same gyromagnetic ratio μ, coupled by a magnetic dipolar interaction. In a time-dependent magnetic field $\mathbf{B}(t)=[B_x(t),B_y(t),B_z]$, the Hamiltonian of this system reads ($\hbar=1$),

$$\hat{\mathsf{H}}(t)=\hat{\mathsf{H}}_0+\mu\mathbf{B}(t)\cdot(\hat{\mathbf{S}}_1+\hat{\mathbf{S}}_2), \tag{1}$$

where

$$\hat{\mathsf{H}}_0=4\xi\hat{S}_1^z\otimes\hat{S}_2^z-\xi(\hat{S}_{1+}\otimes\hat{S}_{2-}+\hat{S}_{1-}\otimes\hat{S}_{2+}) \tag{2}$$

is the part describing the magnetic dipolar spin-spin interaction, with ξ the magnetic dipolar interaction constant, $\hat{\mathbf{S}}_k=[\hat{S}_k^x,\hat{S}_k^y,\hat{S}_k^z]$ the kth spin operator ($k=1,2$), and $\hat{S}_{k\pm}=\hat{S}_k^x\pm i\hat{S}_k^y$. We assume that the static magnetic field B_z in the z

*Email address: sguerin@u-bourgogne.fr

†Present address: Institute of Physics, National Academy of Sciences of Ukraine, prospekt Nauky, 46, 06350, Kiev-39, Ukraine.

direction is strong enough ($|\mu B_z| \gg |\xi|$) so that the Hamiltonian $\hat{\mathsf{H}}_0$ (2) is justified for this case of identical gyromagnetic ratio μ.

We first construct the general equivalent three-level model driven by external fields and next derive the approximate Hamiltonian that takes into account the bichromatic effects by improving the standard rotating wave approximation.

We remark that the effective Hamiltonian we obtain in Eq. (11) applies also to a spin interaction of the form $\hat{\mathsf{H}}_0' = 4\zeta \hat{S}_1^z \otimes \hat{S}_2^z$.

A. The three-level model

In the spin product state space $\{|m\rangle_1 |m\rangle_2\}$ $(m=\downarrow,\uparrow)$, where the states $|\downarrow\rangle_k$ and $|\uparrow\rangle_k$ denote, respectively, the spin-down and spin-up states of the kth spin, a complete basis of orthonormalized eigenstates of $\hat{\mathsf{H}}_0$ is given by

$$|\downarrow\downarrow\rangle \equiv |\downarrow\rangle_1 |\downarrow\rangle_2, \tag{3a}$$

$$|\downarrow\uparrow^+\rangle \equiv \frac{1}{\sqrt{2}}[|\downarrow\rangle_1|\uparrow\rangle_2 + |\uparrow\rangle_1|\downarrow\rangle_2], \tag{3b}$$

$$|\uparrow\uparrow\rangle \equiv |\uparrow\rangle_1 |\uparrow\rangle_2, \tag{3c}$$

$$|\downarrow\uparrow^-\rangle \equiv \frac{1}{\sqrt{2}}[|\downarrow\rangle_1|\uparrow\rangle_2 - |\uparrow\rangle_1|\downarrow\rangle_2]. \tag{3d}$$

In this basis, the Hamiltonian (1) with $\hat{\mathsf{H}}_0$ of Eq. (2) can be exactly expressed in the block-matrix form

$$\mathsf{H}(t) = \begin{bmatrix} \mathsf{H}_c(t) & \mathbf{0} \\ \mathbf{0} & 0 \end{bmatrix}, \tag{4}$$

where

$$\mathsf{H}_c = \begin{bmatrix} \xi - \beta_z & \frac{1}{\sqrt{2}}(\beta_x + i\beta_y) & 0 \\ \frac{1}{\sqrt{2}}(\beta_x - i\beta_y) & -2\xi & \frac{1}{\sqrt{2}}(\beta_x + i\beta_y) \\ 0 & \frac{1}{\sqrt{2}}(\beta_x - i\beta_y) & \xi + \beta_z \end{bmatrix} \tag{5}$$

with $\beta \equiv [\beta_x, \beta_y, \beta_z] = \mu \mathbf{B}$. The state $|\downarrow\uparrow^-\rangle$ is thus decoupled from the other states; it describes the evolution of a spin-0 singlet in a time-dependent magnetic field. This decoupling justifies our choice of the basis. The other three states $|\downarrow\downarrow\rangle$, $|\downarrow\uparrow^+\rangle$, and $|\uparrow\uparrow\rangle$ are coupled by the transverse (xy) magnetic field. To complete the definition of the problem, we suppose that initially the two-spin system is in the unentangled state $|\downarrow\downarrow\rangle$. Our goal is to establish the conditions leading to the most efficient robust transfer into the entangled state $|\downarrow\uparrow^+\rangle$.

We consider the case when the spin system interacts with a constant magnetic field in the z direction and two radio-frequency fields of respective frequencies ω_1 and ω_2 in the x direction,

$$\beta_z = \text{const}, \tag{6a}$$

$$\beta_x = \Omega_1(t)\cos(\omega_1 t + \theta_1) + \Omega_2(t)\cos(\omega_2 t + \theta_2), \tag{6b}$$

$$\beta_y = 0, \tag{6c}$$

where we assume positive Ω_1 and Ω_2. The state vector $\phi(t)$ is solution of the Schrödinger equation $i(d/dt)\phi(t) = \mathsf{H}_c(t)\phi(t)$ with the Hamiltonian $\mathsf{H}_c(t)$ (5) written in the basis $\{|\downarrow\downarrow\rangle, |\downarrow\uparrow^+\rangle, |\uparrow\uparrow\rangle\}$. When the radio-frequency fields are off $(\beta_x = 0))$, we have thus the following energies $E_{\downarrow\downarrow} \equiv \xi - \beta_z$, $E_{\downarrow\uparrow^+} \equiv -2\xi$, and $E_{\uparrow\uparrow} \equiv \xi + \beta_z$. Without loss of generality we assume $\xi < 0$ and $\beta_z > 0$, leading for a strong enough static magnetic field B_z such that $\beta_z = \mu B_z > 3|\xi|$ to a ladder configuration $E_{\downarrow\downarrow} < E_{\downarrow\uparrow^+} < E_{\uparrow\uparrow}$, whose anharmonicity is given by

$$a \equiv [(E_{\uparrow\uparrow} - E_{\downarrow\uparrow^+}) - (E_{\downarrow\uparrow^+} - E_{\downarrow\downarrow})]/2 = 3\xi. \tag{7}$$

We apply near resonant fields $\omega_1 \approx E_{\downarrow\uparrow^+} - E_{\downarrow\downarrow}$, $\omega_2 \approx E_{\uparrow\uparrow} - E_{\downarrow\uparrow^+}$, i.e., with the detunings Δ_1 and Δ_2,

$$\omega_1 \equiv -3\xi + \beta_z - \Delta_1, \tag{8a}$$

$$\omega_2 \equiv 3\xi + \beta_z - \Delta_2. \tag{8b}$$

B. The bichromatic rotating wave approximation

According to the RWA, one can neglect nonresonant counter-rotating terms under the conditions $\omega_{1,2} \gg \Omega_{1,2}$. The rotating wave transformation

$$\mathsf{R} = \begin{bmatrix} e^{-iE_{\downarrow\downarrow}t} & 0 & 0 \\ 0 & e^{-i(E_{\downarrow\downarrow}+\omega_1)t} & 0 \\ 0 & 0 & e^{-i(E_{\downarrow\downarrow}+\omega_1+\omega_2)t} \end{bmatrix} \tag{9}$$

leads to the state vector $\tilde{\phi}(t) = \mathsf{R}^\dagger \phi(t)$ (whose coefficients have the same absolute values as the ones of ϕ) that satisfies the Schrödinger equation

$$i\frac{d}{dt}\tilde{\phi}(t) = \tilde{\mathsf{H}}_c(t)\tilde{\phi}(t), \tag{10}$$

with the Hamiltonian $\tilde{\mathsf{H}}_c = \mathsf{R}^\dagger \mathsf{H}_c \mathsf{R} - i(\partial \mathsf{R}^\dagger/\partial t)\mathsf{R}$, where only the quasiresonant terms have been kept,

$$\tilde{\mathsf{H}}_c = \frac{1}{2}\begin{bmatrix} 0 & \Omega_1 & 0 \\ \Omega_1 & 2\Delta_1 & \Omega_2 \\ 0 & \Omega_2 & 2(\Delta_1+\Delta_2) \end{bmatrix} + \frac{1}{2}\begin{bmatrix} 0 & e^{-i\delta t}\Omega_2 & 0 \\ e^{i\delta t}\Omega_2 & 0 & e^{i\delta t}\Omega_1 \\ 0 & e^{-i\delta t}\Omega_1 & 0 \end{bmatrix}. \tag{11}$$

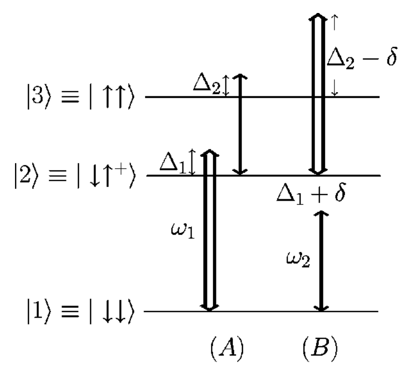

FIG. 1. Diagram of linkage patterns between the three states showing the different couplings. Note that Δ_1 and Δ_2 have been chosen negative here.

The frequency

$$\delta \equiv \omega_1 - \omega_2 = -6\xi + \Delta_2 - \Delta_1 \tag{12}$$

characterizes the *coupling ambiguity* [8]. Note that the standard RWA, for which $\Omega_1, \Omega_2 \ll |\delta|$, corresponds to keeping only the first term in the Hamiltonian (11) if the field 1 (field 2) is resonant with the 1-2 transition (2-3 transition). The full Hamiltonian $\tilde{\mathsf{H}}_c$ allows both fields to couple the two transitions when the field amplitudes Ω_1 and Ω_2 are not small compared to $|\delta|$. The competing coupling schemes are depicted in Fig. 1 . Two limit channels can thus be exhibited, each of which can be given by a standard RWA: the channel A shown in the left part of Fig. 1 (channel B shown in right part of Fig. 1) corresponds to the situation when the field 1 (field 2) couples *only* the 1-2 transition and the field 2 (field 1) couples *only* the 2-3 transition.

The standard RWA can be made if $\Omega_{\max} \ll |a|$, where $\Omega_{\max}$ is the peak Rabi frequency for Ω_i, $i=1,2$. Furthermore, adiabatic passage will require the standard condition $\Omega_{\max}\tau \gg 1$, where τ represents the time of interaction. A standard weak interaction ξ of the order of 100 Hz will thus require a time of interaction of the order of 1 s to satisfy both the RWA and the adiabatic passage condition, which is of the order of the spin relaxation time. Thus a weak interaction requires to take into account the bichromatic effects (with a larger peak Rabi frequency to shorten the time of interaction) in order to avoid the relaxation effects.

We will study more precisely in Secs. V and VI the various regimes that occur in this system. The problem of preparing the entangled state $|2\rangle \equiv |\downarrow\uparrow^+\rangle$ is thus reduced to the study of the population transfer into the intermediate level in the ladder system driven by the Hamiltonian $\tilde{\mathsf{H}}_c$ (11).

The populations given by the Schrödinger equation (10) are invariant under the following transformation $\mathcal{T}$:

$$\Delta_1 \rightarrow \Delta_1 + \delta, \tag{13a}$$

$$\Delta_2 \rightarrow \Delta_2 - \delta, \tag{13b}$$

$$\delta \rightarrow -\delta, \tag{13c}$$

$$\Omega_1 \rightleftharpoons \Omega_2. \tag{13d}$$

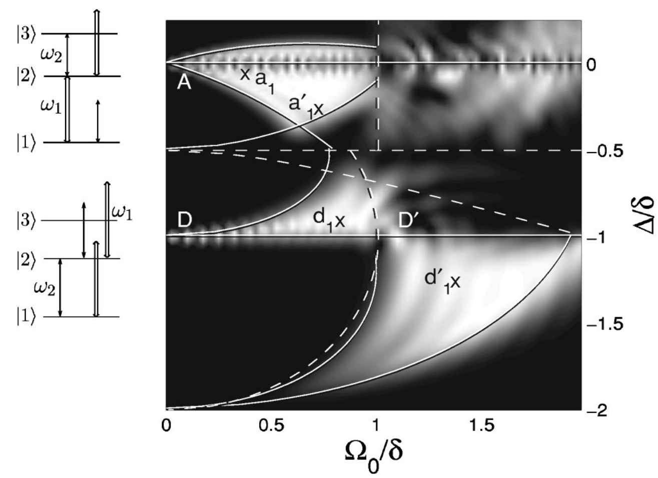

FIG. 2. Contour map of population transfer efficiency $P_2(\infty)$ for varying peak Rabi frequency Ω_0/δ and varying detuning Δ/δ (with $\Delta = \Delta_1 = \Delta_2$) for the sequence 1. White areas correspond to high efficiency transfer (close to 1) to the entangled state. Dark areas correspond to low efficiency transfer (close to 0) to the entangled state $|2\rangle$. The dashed lines separate different regions labeled A, D, and D', associated with different effective Hamiltonians constructed in Secs. V and VI. The regimes of good population transfer are bounded by full lines predicted from the topological analysis. The crosses labeled (a_1), (a'_1), (d_1), and (d'_1) refer to parameters leading to high efficiency. They also refer to the pathways shown, respectively, in Figs. 6, 7, 8, and 9. Besides regions A and D, we have displayed the corresponding linkage patterns, respectively, for $\Delta = 0$ and $\Delta = -\delta$.

We indeed obtain $\tilde{\mathsf{R}}^\dagger(\mathcal{T}\tilde{\mathsf{H}}_c)\tilde{\mathsf{R}} - i(\partial\tilde{\mathsf{R}}^\dagger/\partial t)\tilde{\mathsf{R}} = \tilde{\mathsf{H}}_c$, with the unitary transformation

$$\tilde{\mathsf{R}} = \begin{bmatrix} 1 & 0 & 0 \\ 0 & e^{-i\delta t} & 0 \\ 0 & 0 & 1 \end{bmatrix}. \tag{14}$$

III. NUMERICAL RESULTS

In this section, we describe the numerical results that are obtained by solving the Schrödinger equation (10), for which we will present a detailed theoretical analysis in the following sections.

Figures 2 and 3 display the population of the state $|2\rangle$ at the end of a sequence of delayed Gaussian pulses of the same lengths and the same peak amplitudes,

$$\Omega_1(t) = \Omega_0 \exp[-(t+\tau)^2/T^2], \tag{15a}$$

$$\Omega_2(t) = \Omega_0 \exp[-(t-\tau)^2/T^2], \tag{15b}$$

for various normalized peak amplitudes Ω_0/δ and detunings Δ/δ, where we have chosen

$$\Delta \equiv \Delta_1 = \Delta_2. \tag{16}$$

We have considered this restriction of the parameters because it gives preferentially large regions of good population

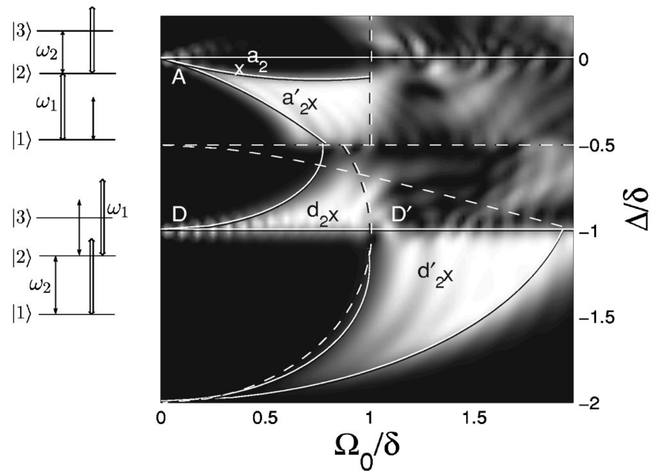

FIG. 3. Contour map of population transfer efficiency $P_2(\infty)$ for varying peak Rabi frequency Ω_0/δ and varying detuning Δ/δ for the sequence 2. The cross labeled (a_2) in one region of low efficiency and the ones labeled (a_2'), (d_2), and (d_2') in the regions of high efficiency refer to the pathways shown, respectively, in Figs. 6, 7, 8, and 9.

transfer. This will be justified in Secs. V and VI. Note that the case $\Delta_1=-\Delta_2$ is irrelevant since it corresponds to a two-photon resonance between the product states $|\downarrow\downarrow\rangle$ and $|\uparrow\uparrow\rangle$. We could have considered equivalently the restriction $\Delta_2=\Delta_1+2\delta$ in accordance with the symmetry (13). The two possible orderings of pulses have been considered: the sequence 1 of Fig. 2 (the sequence 2 of Fig. 3) corresponds to the ω_1 pulse (the ω_2 pulse) being switched on first, with the delay $\tau=1.7T$ ($\tau=-1.7T$). Global adiabaticity is ensured by the choice of a large pulse area $\Omega_0 T=50$.

One can distinguish three islands of robust high transfer (white regions). Specific parameters characterizing these islands are labeled by (a), (a'), (d), and (d'), with the subscript 1 or 2, respectively, for Figs. 2 or 3 [except (a_2) which is outside the regions of high transfer]. These islands of high transfer are analyzed in the following sections by using the dressed Hamiltonian corresponding to $\tilde{\mathsf{H}}_c$ (11) and the adiabatic properties of the dynamics. We will characterize different regimes and associate them with different effective dressed Hamiltonians. We will show that the islands of good transfer can be understood from the topological properties of the appropriate effective dressed Hamiltonian.

We will show the following results.

(i) Regions (a) correspond to a STIRAP-like process associated with the channel A (see Fig. 1) that is perturbed (in the sense of non-resonant perturbation theory) by the channel B. Note that the restriction $\Delta_2=\Delta_1+2\delta$ would have given a STIRAP-like process associated with the channel B perturbed by the channel A.

(ii) Regions (d) (in the weak field regime, i.e., $\Omega_1,\Omega_2<|\delta|$) correspond to an effective two-level SCRAP-like (Stark chirped rapid adiabatic passage) process [9,10].

(iii) Regions (d') (in the strong field regime, i.e., $\Omega_1,\Omega_2\gtrsim|\delta|$) correspond to an effective two-level bichromatic SCRAP process (with additional Stark shifts) as described in Ref. [11].

IV. THE FLOQUET DRESSED HAMILTONIAN

In this section we derive the Floquet Hamiltonian describing the full Hamiltonian of the spin system dressed by the strong fields. It will allow to predict and interpret the various processes occurring in this system by adiabatic passage.

It is convenient to use the adiabatic Floquet theory in order to study the Hamiltonian $\tilde{\mathsf{H}}_c$ (11) since its time dependence contains a characteristic frequency δ. The Floquet Hamiltonian corresponding to $\tilde{\mathsf{H}}_c$ is [8,13]

$$\mathsf{K}^{[\Omega_1,\Omega_2]}=-i\hbar\delta\frac{\partial}{\partial\theta}+\frac{1}{2}\begin{bmatrix}0 & \Omega_1+e^{-i\theta}\Omega_2 & 0\\ \Omega_1+e^{i\theta}\Omega_2 & 2\Delta_1 & \Omega_2+e^{i\theta}\Omega_1\\ 0 & \Omega_2+e^{-i\theta}\Omega_1 & 2(\Delta_1+\Delta_2)\end{bmatrix}. \quad (17)$$

We have formulated this Floquet Hamiltonian in a way which derives naturally from the theory of quantized dressed states in a cavity [12]. The Floquet Hamiltonian allows to take into account the photon exchanges between the atom and the fields. It is formally constructed on the initial phases θ_1 and θ_2 of the fields which are treated as dynamical variables acting on the photonic Hilbert space $\mathcal{L}=\mathcal{L}_2(d\theta_1/2\pi)\otimes\mathcal{L}_2(d\theta_2/2\pi)$, where each $\mathcal{L}_2(d\theta_i/2\pi)$ is the Hilbert space of 2π-periodic functions of the angle θ_i [11]. Since we have applied a bichromatic rotating wave approximation, only the frequency $\delta=\omega_1-\omega_2$, associated with the dynamical variable $\theta\equiv\theta_1-\theta_2$ is left in the effective Hamiltonian. The effective Floquet Hamiltonian K (17) acts thus on the Hilbert space spanned by the three states $\{|1\rangle,|2\rangle,|3\rangle\}$ tensored by the effective photonic Hilbert space $\mathcal{L}_2(d\theta/2\pi)$. This photonic Hilbert space allows to take into account the exchanges of the group of ω_1-ω_2 photons. The eigenstates of K are families of three states denoted $|1;k,-k\rangle$, $|2;k-1,-k\rangle$, and $|3;k-1,-k-1\rangle$ with k a positive or negative integer. The corresponding eigenvalues $\lambda_{1;k,-k}$, $\lambda_{2;k-1,-k}$ and $\lambda_{3;k-1,-k-1}$ have the following periodicity property: $\lambda_{n;k_1,k_2}=\lambda_{n;k_1-1,k_2+1}+\hbar\delta$, for $n=1,2,3$. The notation $|n;k_1,k_2\rangle$ characterizes (when the fields are off) the state $|n\rangle$ dressed by the field of k_1 ω_1 photons and of k_2 ω_2 photons. The integers k_1 and k_2 characterize thus relative photon numbers of the respective fields of frequency ω_1 and ω_2. The initial state is denoted $|1;0,0\rangle$. The problem can be formulated as follows: *we look for robust adiabatic connections between the initial state* $|1;0,0\rangle$ *and the final state* $|2;k-1,-k\rangle$ *for some positive or negative integer k.*

The Floquet Hamiltonian (17) depends parametrically on the pulse shapes and the detunings. The possible connections depend on the *topology* of the eigenenergy surfaces of Eq. (17) as functions of the field envelopes Ω_1 and Ω_2 for given detunings Δ_1 and Δ_2 [11,14]. The topology is characterized by true crossings which occur generically when one of the fields is off. We will study in the following the topology of K using different effective dressed Hamiltonians corresponding

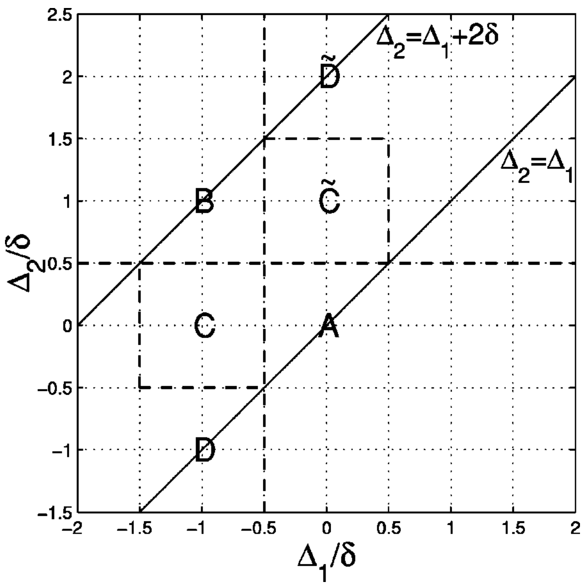

FIG. 4. Schematic diagram of the regimes for a weak-field regime as a function of the normalized detunings Δ_1/δ and Δ_2/δ. The restriction $\Delta_2=\Delta_1$ has been used for Figs. 2 and 3.

to different regimes. These regimes will depend on the ranges of the detunings and of the field amplitudes.

In the next sections we will calculate the eigenenergy surfaces for different relevant cases, using a numerical diagonalization of Eq. (17). This can be done either by discretization of the angle θ or equivalently by using a restricted finite basis of the complete basis $\{e^{ik\theta},k\in\mathbb{Z}\}$ of the photonic Hilbert space $\mathcal{L}_2(d\theta/2\pi)$. Effective Hamiltonians will be determined in the appropriate regions, which give good approximations for these numerical surfaces, and provide an analytic explanation of the different domains where adiabatic transfer is efficient.

We classify the different regimes and construct effective dressed Hamiltonians by determining in the Hamilonian K (17) which terms are *resonant* (or *quasiresonant*) and which are only *perturbative*. The resonant terms are treated by an adapted unitary transformation which allows an explicit diagonalization, whereas the perturbative terms can be treated by stationary pertubation theory. This technique has been presented in Ref. [15]. Note that for a simple RWA two-level system of Rabi frequency Ω and detuning Δ, the perturbative regime is such that $\Omega\ll|\Delta|$ and the resonant regime such that $\Omega\gtrsim|\Delta|$. We classify the different regimes as functions of the ranges of the field amplitudes and of the detunings.

In the following, we have normalized all the quantities with respect to δ.

V. WEAK-FIELD REGIME

The *weak-field regime* occurs when $\Omega_1(t),\Omega_2(t)<\delta$. Note that when one has $\Delta_1=\Delta_2$ additionally, this regime coincides with a *strong spin coupling* since we have then $6|\xi|>\Omega_1(t),\Omega_2(t)$. In this case of weak-field regime, we can intuitively analyze the different regimes with respect to the range of the detunings using the diagram of linkage patterns (Fig. 1). Six relevant regimes (bounded by dashed lines) have been collected in Fig. 4, depending on the quasiresonances.

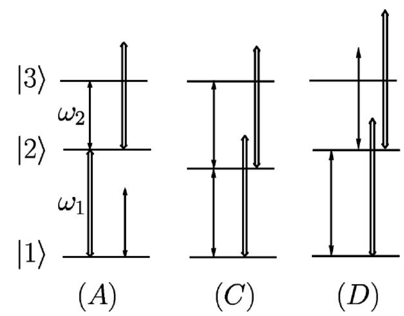

FIG. 5. Diagram of linkage patterns for the three regimes (in the resonant case): A ($\Delta_1=\Delta_2=0$), C ($\Delta_1=-\delta,\Delta_2=0$), and D ($\Delta_1=-\delta,\Delta_2=-\delta$).

(A) The transition 1-2 is quasiresonant with ω_1 and perturbed by ω_2, 2-3 is quasiresonant with ω_2 and perturbed by ω_1.

(B) 1-2 is quasiresonant with ω_2 and perturbed by ω_1, 2-3 is quasiresonant with ω_1 and perturbed by ω_2.

(C) 1-2 and 2-3 are both quasiresonant with ω_2, and perturbed by ω_1.

(D) 1-2 is quasiresonant with ω_2 and perturbed by ω_1, 2-3 is perturbed by ω_2 and ω_1.

($\tilde{C}$) 1-2 and 2-3 are both quasiresonant with ω_1, and perturbed by ω_2.

($\tilde{D}$) 1-2 is quasiresonant with ω_1 and perturbed by ω_2, 2-3 is perturbed by ω_1 and ω_2.

In the exact resonant cases, we have represented the regimes A, C, and D in Fig. 5.

As shown schematically in Fig. 4, the above regimes can be roughly bounded by

$$\Delta_1=\pm\delta/2,\quad \Delta_1=-3\delta/2,\quad \Delta_2=\pm\delta/2,\quad \Delta_2=3\delta/2. \tag{18}$$

By the symmetry (13), we recover the regime B from the regime A, $\tilde{C}$ from C, $\tilde{D}$ from D (exchanging additionally Ω_1 and Ω_2).

The regimes A and B are STIRAP-like regimes; D and $\tilde{D}$ are SCRAP-like regimes.

We do not consider other regimes where the state $|1\rangle$ is almost not depopulated by adiabatic passage.

The line $\Delta=-\delta/2$ appears as a dashed line in Figs. 2 and 3, where the restriction $\Delta_1=\Delta_2$ has been considered.

A. Regime A

When the transition 1-2 is quasiresonant with the frequency ω_1 and the transition 2-3 quasiresonant with the frequency ω_2, the process can be analyzed as the channel A *perturbed* (in the sense nonresonant perturbation theory) by the channel B. We refer to it as the regime A as shown in Figs 2 and 3, where it is roughly bounded by the dashed lines $\Delta=-\delta/2$, $\Delta=\delta/2$ (not shown), and $\Omega_0=\delta$. This regime is approximately characterized by the following effective Hamiltonian in the basis $\{|1;0,0\rangle, |2;-1,0\rangle, |3;-1,-1\rangle\}$ [13]:

$$\tilde{\mathsf{H}}_c^{\mathrm{A}}=\frac{1}{2}\begin{bmatrix} -\frac{(\Omega_2)^2}{2(\delta+\Delta_1)} & \Omega_1 & 0 \\ \Omega_1 & 2\Delta_1+\frac{(\Omega_2)^2}{2(\delta+\Delta_1)}+\frac{(\Omega_1)^2}{2(\delta-\Delta_2)} & \Omega_2 \\ 0 & \Omega_2 & 2(\Delta_1+\Delta_2)-\frac{(\Omega_1)^2}{2(\delta-\Delta_2)} \end{bmatrix}, \tag{19}$$

which corresponds to the Hamiltonian characterizing the channel A with additional time dependent Stark shifts (on the diagonal) induced by the channel B. Note that this effective Hamiltonian is less precise for bigger Ω_1 or Ω_2 approaching δ.

1. Topology of the channel A in the RWA limit

Before analyzing the dynamics given by this Hamiltonian (19), we recall the results in the limit case of a very weak-field $\Omega_1(t),\Omega_2(t)\ll\delta$ obtained in Ref. [14]. In this case the perturbative terms can be neglected and the Hamiltonian becomes

$$\tilde{\mathsf{H}}_c^{A}\to\frac{1}{2}\begin{bmatrix} 0 & \Omega_1 & 0 \\ \Omega_1 & 2\Delta_1 & \Omega_2 \\ 0 & \Omega_2 & 2(\Delta_1+\Delta_2) \end{bmatrix}. \tag{20}$$

This resulting effective Hamiltonian corresponds to the channel A alone. The topology of the energy surfaces of this Hamiltonian has been analyzed in Ref. [14]. It has been shown that the adiabatic transfer to state $|2\rangle$ is topologically allowed for

$$\Delta_1\Delta_2>0. \tag{21}$$

The topological analysis shows moreover that for the sequence 1 the region of this process is bounded in the parameter space by the curves

$$\Omega_0=2\sqrt{\Delta_1(\Delta_1+\Delta_2)} \tag{22}$$

and for the sequence 2 by the curves (22) and

$$\Omega_0=2\sqrt{\Delta_2(\Delta_1+\Delta_2)}. \tag{23}$$

2. Topology of the channel A perturbed by the channel B

Taking now into account the perturbation by the channel B [Hamiltonian (19)] leads to two kinds of topology as shown in Figs. 6 and 7, where the surfaces of quasienergies as functions of the normalized Rabi frequencies Ω_1/δ and Ω_2/δ, respectively, for $\Delta=\Delta_1=\Delta_2=-\delta/20$ and $\Delta=\Delta_1=\Delta_2=-\delta/4$ have been displayed. The eigenvalues of Eq. (19) (not shown) fit these surfaces well except in Fig. 7 when $\Omega_1\sim\delta$ and $\Omega_2\sim\delta$ because of an additional dynamical resonance (i.e., a resonance occuring beyond a threshold of the field amplitudes) [15,8] which involves the surface connected with $|3;0,-2\rangle$ (which corresponds to the surface connected to $|3;-1,-1\rangle$ and translated of δ) and the surface right below.

Figure 6 shows that the two conical intersections, one occurring for $\Omega_1=0$, the other one for $\Omega_2=0$, determine the boundary of the adiabatic connection between the initial state $|1;0,0\rangle$ and the target state $|2;-1,0\rangle$. A detailed analysis of the dynamics through the conical intersections can be found in Ref. [14]. We summarize here the main results using an example of a crossing occurring for $\Omega_1=0$: if the dynamics goes *exactly* through the crossing, where Ω_1 is exactly zero, then adiabatic passage through the intersection occurs along

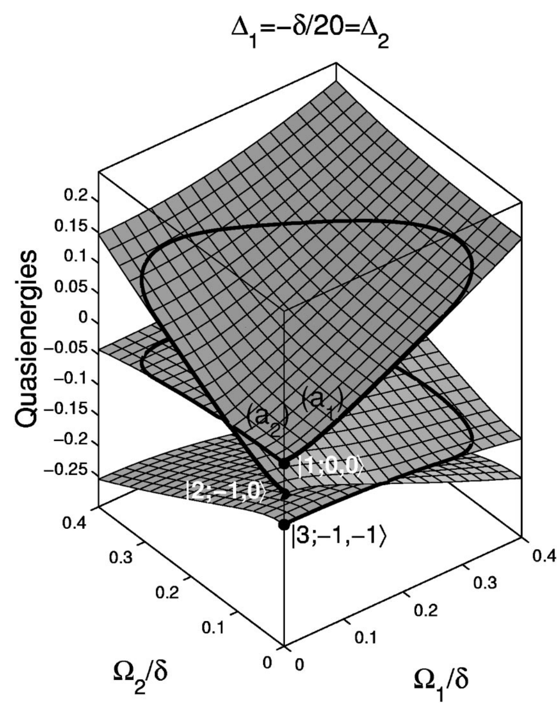

FIG. 6. Quasienergy surfaces (in units of δ) as functions of Ω_1/δ and Ω_2/δ for $\Delta_1=\Delta_2=-\delta/20$. The path denoted a_1 (sequence 1), for $\Omega_0=0.35\delta$, connects the states $|1\rangle$ and $|2\rangle$ with the absorption of one ω_1 photon. The path denoted a_2 (sequence 2), for $\Omega_0=0.35\delta$, connects the states $|1\rangle$ and $|3\rangle$ with the absorptions of one ω_1 photon and of one ω_2 photon.

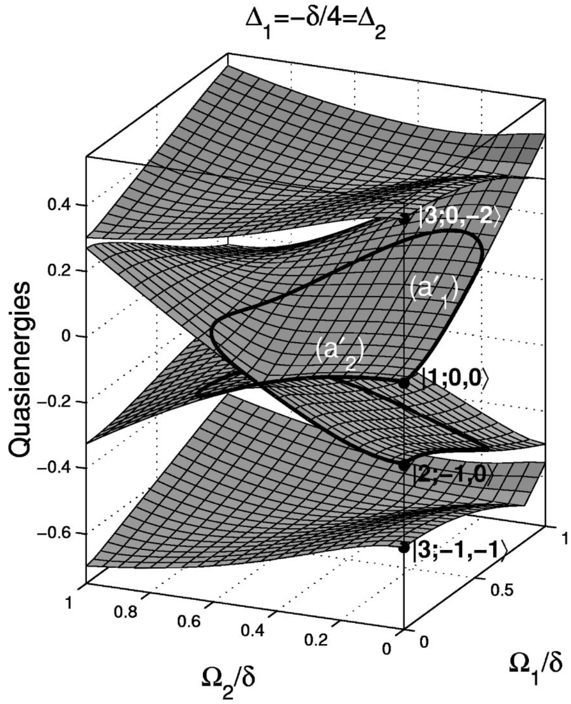

FIG. 7. Quasienergy surfaces as functions of Ω_1/δ and Ω_2/δ for $\Delta_1=\Delta_2=-\delta/4$. The two different paths, denoted a_1' and a_2' (for $\Omega_0=0.7\delta$) depending on the sequence of the pulses connect the states $|1\rangle$ and $|2\rangle$ with the absorption of one ω_1 photon.

a smooth line. If the dynamics slightly misses the crossing, i.e., for a specific $\Omega_1\neq 0$, it encounters instead a thin avoided crossing. It is expected to be passed *diabatically*, i.e., with a jump from one branch to the other, for a sufficiently small Ω_1 with respect to the speed of the passage, according to a local Landau-Zener analysis. Thus the Landau-Zener analysis provides the matching between the adiabatic evolution far from the conical intersection and the diabatic behavior near the intersection. Note that a too large Ω_1 with respect to the speed of the passage would lead either (i) to an undesirable splitting of the population along the two surfaces near the intersection, followed by an adiabatic evolution of these two states, or (ii) for a larger Ω_1, to an adiabatic evolution staying on the initial surface.

For the sequence 1, the conical intersection occurring for $\Omega_1=0$ is favorable for this adiabatic connectivity. The path denoted a_1 (also corresponding to the cross a_1 of Fig. 2) is an example for the complete transfer. However, for the sequence 2, the conical intersection occurring for $\Omega_1=0$ is also favorable but the one occurring for $\Omega_2=0$ is detrimental since it makes $|1;0,0\rangle$ connect to $|3;-1,-1\rangle$. The path denoted a_2 is an example for the complete transfer to $|3;-1,-1\rangle$ (also corresponding to the cross a_2 of Fig. 3).

For a bigger detuning (in absolute value), the topology is different as shown in Fig. 7. The previous conical intersection occurring for $\Omega_2=0$ has now disappeared and another one involving the surfaces connected to $|1;0,0\rangle$ and $|3;0,-2\rangle$ has appeared. The two conical intersections, the one occurring for $\Omega_1=0$ and the other one for $\Omega_2=0$, are involved for the adiabatic connection between the initial state $|1;0,0\rangle$ and the target state $|2;-1,0\rangle$. More precisely, for the sequence 1, these two conical intersections determine the boundary of this adiabatic connection; the path denoted a_1' (also corresponding to the cross a_1' of Fig. 2) is an example for the complete transfer. However, for the sequence 2 only the conical intersection occurring for $\Omega_1=0$ binds now the adiabatic connection; the path denoted a_2' is an example for the complete transfer (also corresponding to the cross a_2' of Fig. 3).

Using the effective Hamiltonian (19), the position of the previous conical intersections, for $\Omega_1=0$ and $\Omega_2=0$, respectively, lead to the three boundaries for the sequence 1,

$$\Delta=\frac{\Omega_2}{16\delta}[-5\Omega_2\pm\sqrt{9(\Omega_2)^2+32\delta^2}], \tag{24a}$$

$$\Omega_1=\sqrt{2(\delta-\Delta)[2(\delta+\Delta)-\sqrt{2(\delta+\Delta)}]}. \tag{24b}$$

The delay between the pulses has been chosen sufficiently large such that it is a good approximation to consider that the adiabatic connectivity is quite well described by the value of the peak amplitudes. Thus we have displayed these boundaries in Fig. 2 as full lines, with $\Omega_2=\Omega_0$ for Eq. (24a) and with $\Omega_1=\Omega_0$ for Eq. (24b). They globally determine the boundary of the lower and upper part of the island of good transfer of the regime A observed in the numerical computation. This island is crossed by the line of resonance $\Delta=0$ around which the transfer to $|2\rangle$ depends on the pulse areas, as shown by small oscillating islands.

For the sequence 2, the conical intersections involved give the following boundaries:

$$\Delta=\frac{\Omega_2}{16\delta}[-5\Omega_2-\sqrt{9(\Omega_2)^2+32\delta^2}], \tag{25a}$$

$$\Omega_1=\sqrt{(\delta-\Delta)[4\Delta+\delta\pm\sqrt{\delta(\delta+8\Delta)}]},\quad \text{for}\quad \Delta<0. \tag{25b}$$

These curves are displayed in Fig. 3, with $\Omega_2=\Omega_0$ for Eq. (25a) and with $\Omega_1=\Omega_0$ for Eq. (25b). They give a good prediction of the island of good transfer of the regime A observed numerically.

For the two sequences, the islands of good transfer to the state $|2\rangle$ of the regime A occur with absorption of one ω_1 photon.

B. Regime *B*

This regime is characterized by the transition quasiresonant 1-2 with the frequency ω_2 and the quasiresonant transition 2-3 with the frequency ω_1. This process can be analyzed as the channel B *perturbed* (in the sense of nonresonant perturbation theory) by the channel A and is described by the effective Hamiltonian $\tilde{\mathsf{H}}_c^B=\mathcal{T}\tilde{\mathsf{H}}_c^A$,

$$\tilde{\mathsf{H}}_c^{\mathrm{B}}=\frac{1}{2}\begin{bmatrix} -\frac{(\Omega_1)^2}{2\Delta_1} & \Omega_2 & 0 \\ \Omega_2 & 2(\Delta_1+\delta)+\frac{(\Omega_1)^2}{2\Delta_1}-\frac{(\Omega_2)^2}{2\Delta_2} & \Omega_1 \\ 0 & \Omega_1 & 2(\Delta_1+\Delta_2)+\frac{(\Omega_2)^2}{2\Delta_2} \end{bmatrix}. \tag{26}$$

The regions of high transfer efficiency to the state $|2\rangle$ are bounded in the same manner as in the regime A by the lines (24) and (25) to which we apply the transformation $\mathcal{T}$ (13).

C. Regime *C*

The regime *C* is characterized by a mixture of regimes *A* and *B* for which the transitions 1-2 and 2-3 are both quasiresonant with the same frequency ω_2. As long as the ω_1 field is perturbative for both transitions, we have the following effective Hamiltonian:

$$\tilde{\mathsf{H}}_c^{C}=\frac{1}{2}\begin{bmatrix} -\frac{(\Omega_1)^2}{2\Delta_1} & \Omega_2 & 0 \\ \Omega_2 & 2(\Delta_1+\delta)+\frac{(\Omega_1)^2}{2\Delta_1}-\frac{(\Omega_1)^2}{2(\Delta_2-\delta)} & \Omega_2 \\ 0 & \Omega_2 & 2(\Delta_1+\Delta_2+\delta)+\frac{(\Omega_1)^2}{2(\Delta_2-\delta)} \end{bmatrix}, \tag{27}$$

in the basis $\{|1;0,0\rangle, |2;0,-1\rangle, |3;0,-2\rangle\}$. No efficient transfer is observed in this regime.

D. Regime *D*

This regime is such that the only quasiresonance is between the states 1 and 2 with ω_2. In this case, in the basis $\{|1;0,0\rangle, |2;0,-1\rangle, |3;0,-2\rangle\}$ we can construct an effective Hamiltonian from the previous one [Eq. (27)] considering that the ω_2 field is perturbative for the transition 2-3,

$$\tilde{\mathsf{H}}_c^{D}=\frac{1}{2}\begin{bmatrix} -\frac{(\Omega_1)^2}{2\Delta_1} & \Omega_2 & 0 \\ \Omega_2 & 2(\Delta_1+\delta)+\frac{(\Omega_1)^2}{2\Delta_1}-\frac{(\Omega_1)^2}{2(\Delta_2-\delta)}-\frac{(\Omega_2)^2}{2\Delta_2} & 0 \\ 0 & 0 & 2(\Delta_1+\Delta_2+\delta)+\frac{(\Omega_1)^2}{2(\Delta_2-\delta)}+\frac{(\Omega_2)^2}{2\Delta_2} \end{bmatrix}. \tag{28}$$

We can remark that this Hamiltonian is valid for the field amplitude Ω_2 below the position of the resonance occurring between the transition 2-3 and the ω_2 field that can be estimated by

$$\Omega_2^r \equiv 2\sqrt{\Delta_2(\Delta_1+\Delta_2+\delta)} \quad \text{and} \quad \Delta_1+2\Delta_2+\delta \leqslant 0. \tag{29}$$

This limit is represented as the bent dashed line crossing the figure horizontally in Figs. 2 and 3 (with $\Omega_0=\Omega_2^r$). Below this limit, one is allowed to decouple the states $|2;0,-1\rangle$ and $|3;0,-2\rangle$ from the Hamiltonian (27). A more detailed analysis of this regime shows that a *dynamical resonance* between the transition 1-2 and the ω_1 field, induced by the ω_2 field occurs approximately for

$$\Omega_2=\Omega_2^{\mathrm{dr}} \equiv \sqrt{-\Delta_1(\Delta_1+2\delta)}. \tag{30}$$

It is obtained when the difference of the dressed eigenvalues connected to $|1;0,0\rangle$ and $|2;0,-1\rangle$ (calculated without the Stark shifts) compensates the difference of the frequencies δ. This additional resonance is described as dynamical since it occurs beyond a threshold of the ω_2 field amplitude. It is represented as the bent dashed line crossing the figure vertically (which separates the regimes *D* and *D*′) in Figs. 2 and 3 with $\Omega_0=\Omega_2^{\mathrm{dr}}$. The Hamiltonian (28) is thus approximately valid *before* the dynamical resonance (30).

Below this dynamical resonance, this Hamiltonian (28) is very similar to the one describing the Stark chirped rapid adiabatic passage between the states $|1;0,0\rangle$ and $|2;0,-1\rangle$ [9]. The pump of this process is here Ω_2 and the Stark pulse Ω_1. We have here Ω_2 acting additionally as a Stark pulse.

It is important to note that when $\Delta_1=-\delta$, the field ω_2 is exactly in resonance with the transition 1-2, and it cannot induce any complete population transfer from $|1\rangle$ to $|2\rangle$.

Below this boundary (plotted as a full line in Figs. 2 and 3), i.e., for $\Delta_1 < -\delta$, the topology does not allow the transfer from $|1\rangle$ to $|2\rangle$. Above this boundary ($\Delta_1 > -\delta$), the transfer is possible as shown by the surfaces of quasienergies (for $\Delta = \Delta_1 = \Delta_2 = 9\delta/10$) in Fig. 8. The eigenvalues of Eq. (28) (not shown) fit well these surfaces below the dynamical resonances $\Omega_2 < \Omega_2^r$. Figure 8 shows that the conical intersection for $\Omega_2 = 0$ between the surfaces connected to $|1;0,0\rangle$ and the target state $|2;0,-1\rangle$ determines the boundary of the adiabatic connection between these states. This characterizes a transfer to the state $|2\rangle$ with absorption of one ω_2 photon. This boundary is calculated from the effective Hamiltonian (28),

$$\Omega_1 = 2\sqrt{\Delta\frac{\Delta^2-\delta^2}{2\delta-\Delta}}. \tag{31}$$

It is plotted in Figs. 2 and 3 as a full line in the region D and determines the boundary of the upper island of good transfer of this region.

The cases beyond the dynamical resonance are studied in the following section.

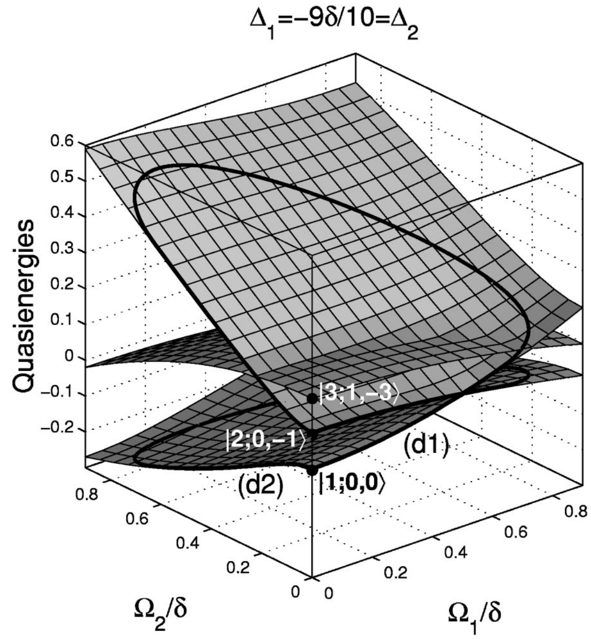

FIG. 8. Quasienergy surfaces as functions of Ω_1/δ and Ω_2/δ for $\Delta_1 = \Delta_2 = -9\delta/10$. Two different paths (denoted d_1 and d_2) for $\Omega_0 = 0.8\delta$ connect the states $|1\rangle$ and $|2\rangle$ with the absorption of one ω_2 photon.

VI. STRONG-FIELD REGIMES

The *strong-field regime* occurs when $\Omega_1(t),\Omega_2(t) \gtrsim \delta$. For $\Delta_1 = \Delta_2$, this corresponds to a *weak spin coupling* since one has then $6|\xi| \lesssim \Omega_1(t),\Omega_2(t)$. More resonances occur in this case and the previous effective Hamiltonians are no longer valid. We will study in detail the interesting regime D' which gives quite large areas of transfer to state $|2\rangle$.

This regime is located below the resonance (29) and beyond the dynamical resonance (30), when the transition 1-2 is quasiresonant with both the ω_1 and ω_2 fields and when the transition 2-3 is not resonant with either the ω_1 field or the ω_2 field. This regime is thus characterized by the effective dressed Hamiltonian,

$$\mathsf{K}^{D'} = -i\delta\frac{\partial}{\partial\theta} + \frac{1}{2}\begin{bmatrix} 0 & \Omega_2 + e^{i\theta}\Omega_1 & 0 \\ \Omega_2 + e^{-i\theta}\Omega_1 & 2(\Delta_1+\delta) - \dfrac{(\Omega_1)^2}{2(\Delta_2-\delta)} - \dfrac{(\Omega_2)^2}{2\Delta_2} & 0 \\ 0 & 0 & 2(\Delta_1+\Delta_2+\delta) + \dfrac{(\Omega_1)^2}{2(\Delta_2-\delta)} + \dfrac{(\Omega_2)^2}{2\Delta_2} \end{bmatrix}. \tag{32}$$

It is equivalent to a two-level system driven by a bichromatic field [11] with additional Stark shifts. The surfaces of quasienergies as functions of the normalized Rabi frequencies Ω_1/δ and Ω_2/δ (for $\Delta = \Delta_1 = \Delta_2 = -7\delta/5$) are displayed in Fig. 9. This figure shows that the two conical intersections, one for $\Omega_1 = 0$ and one for $\Omega_2 = 0$, determine the boundary of the adiabatic connection between the initial state $|1;0,0\rangle$ and the target state $|2;1,-2\rangle$. We calculate the boundaries using the effective Hamiltonian (32), which are plotted as full lines in Figs. 2 and 3,

$$\Omega_1 = 2\sqrt{(\Delta-\delta)[2\delta-\Delta-2\sqrt{\delta(2\delta-\Delta)}]}, \tag{33a}$$

$$\Omega_2 = 2\sqrt{\Delta[\delta-\Delta-\sqrt{\delta(\delta-4\Delta)}]}. \tag{33b}$$

This process corresponds to a multiphoton transfer to the state $|2\rangle$, with absorption of two ω_2 photons and emission of one ω_1 photon.

The analysis of the topology allows to improve the transfer efficiency. It shows indeed that a ω_1 field amplitude weaker than the ω_2 field amplitude is better in this regime since the conical intersection for $\Omega_1 = 0$ occurs for a smaller value than the one for $\Omega_2 = 0$.

This process of a two-level system driven by a bichromatic field studied in Ref. [11] shows that the transfer can still occur for a stronger field (i.e., for a weaker spin coupling), but with absorption of more than two ω_2 photons and emission of more than one ω_1 photon. This result is shown in Fig. 10 where strong field white islands can be observed. The

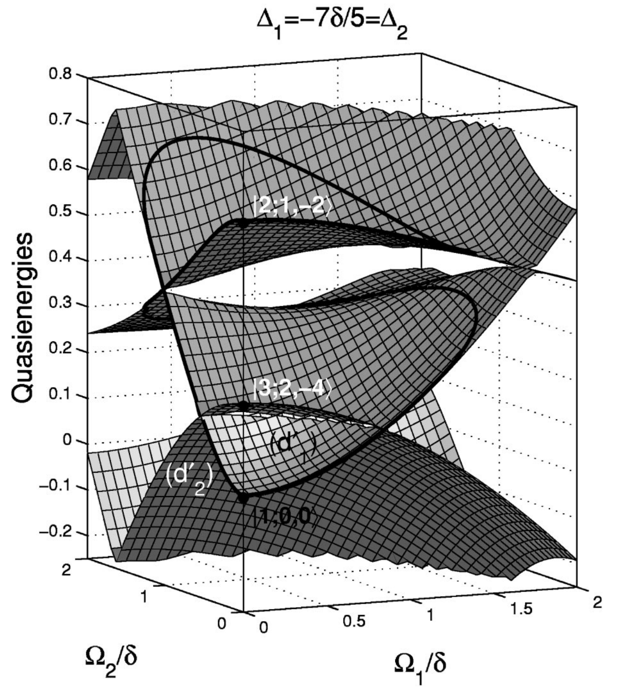

FIG. 9. Quasienergy surfaces as functions of Ω_1/δ and Ω_2/δ for $\Delta_1=\Delta_2=-7\delta/5$. Two different paths (denoted d_1' and d_2') for $\Omega_0=3\delta/2$ connect the states $|1\rangle$ and $|2\rangle$ with the absorption of two ω_2 photons and the emission of one ω_1 photon.

lower white islands correspond to good population transfer to the entangled state $|2;k-1,-k\rangle$, with $k=1,2,3,4$ from left to right.

VII. CONCLUSION

In a system of two interacting identical spins in an external bichromatic field, we have determined the choices of laser pulses which can give a maximal final population in the entangled state. The proposed strategies are robust with respect to the external parameters. We have found that in the parameter space it is possible to find large regions where the quantum system can be transferred to the entangled state with a high efficiency. These regions of good transfer have been characterized by the topology of the surfaces of dressed states as functions of the parameters.

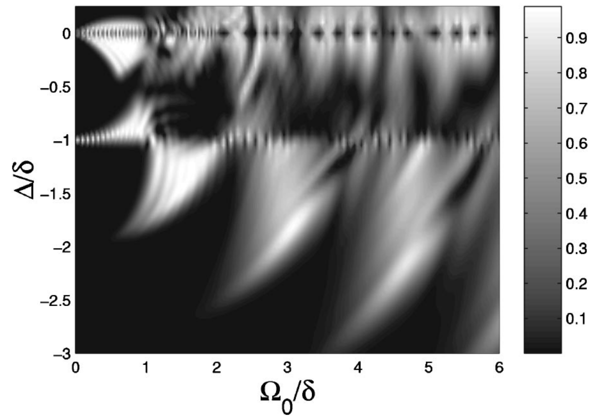

FIG. 10. Contour map of population transfer efficiency $P_2(\infty)$ as in Fig. 2, but for stronger field amplitudes.

The implementation of the scheme we propose in this paper can be realized for different physical systems. An example could be of the type similar to the one used in Ref. [16] for the realization of two-qubit phase gates. The similarity of our model with the nuclear magnetic resonance scheme of Ref. [16] is the adiabatic evolution. The Berry adiabatic phase gate operation was, however, realized for different nuclei i.e. with different gyromagnetic constants. In this case the two-particle states are represented through a four-level quantum system (see, e.g., Ref. [17]). In the present paper we propose instead to use identical spins to generate an entangled state through a simpler effective three-level system.

The methods employed here are quite general and can be applied for a large variety of systems. We anticipate interesting applications of this method in quantum computing and quantum communication.

ACKNOWLEDGMENTS

We acknowledge support by INTAS 99-00019 and the Conseil Régional de Bourgogne. S.G. acknowledges support from a CNRS project ''jeunes chercheurs'' and thanks the Institute of Physics of the National Academy of Sciences of Armenia in Ashtarak for kind hospitality. R.U. thanks for support by the Alexander Von Humboldt Foundation and l'Université de Bourgogne for kind hospitality. The authors thank N. Vitanov for useful discussions.

[1] C. Williams and S. Clearwater, *Explorations in Quantum Computing* (Springer-Verlag, New York, 1998).

[2] E.S. Fry, T. Walther, and S. Li, Phys. Rev. A **52**, 4381 (1995); J.I. Cirac and P. Zoller, Phys. Rev. Lett. **74**, 4091 (1995); E. Hagley, X. Maitre, G. Nogues, C. Wunderlich, M. Brune, J.M. Raimond, and S. Haroche, *ibid.* **79**, 1 (1997); B.E. King, C.S. Wood, C.J. Myatt, Q.A. Turchette, D. Leibfried, W.M. Itano, C. Monroe, and D.J. Wineland, *ibid.* **81**, 1525 (1998); Q.A. Turchette, C.S. Wood, B.E. King, C.J. Myatt, D. Leibfried, W.M. Itano, C. Monroe, and D.J. Wineland, *ibid.* **81**, 3631 (1998).

[3] A. Sørensen and K. Mølmer, Phys. Rev. Lett. **82**, 1971 (1999); C.A. Sackett, D. Kielpinski, B.E. King, C. Langer, C.J. Myatt, M. Rowe, Q.A. Turchatte, W.M. Itano, D.J. Wineland, and C. Monroe, Nature (London) **404**, 256 (2000).

[4] N.V. Vitanov, M. Fleischhauer, B.W. Shore, and K. Bergmann, Adv. At., Mol., Opt. Phys. **46**, 55 (2001).

[5] T. Pellizzari, S.A. Gardiner, J.I. Cirac, and P. Zoller, Phys. Rev. Lett. **75**, 3788 (1995).

[6] I.V. Bargatin, B.A. Grishanin, and V.N. Zadkov, Phys. Rev. A **61**, 052305 (2000).

[7] R. Unanyan, N.V. Vitanov, and K. Bergmann, Phys. Rev. Lett.

87, 137902 (2001).

[8] R.G. Unanyan, S. Guérin, B.W. Shore, and K. Bergmann, Eur. Phys. J. D **8**, 443 (2000).

[9] L.P. Yatsenko, B.W. Shore, T. Halfmann, K. Bergmann, and A. Vardi, Phys. Rev. A **60**, R4237 (1999).

[10] T. Rickes, L.P. Yatsenko, S. Steuerwald, T. Halfmann, B.W. Shore, N.V. Vitanov, and K. Bergmann, J. Chem. Phys. **113**, 534 (2000).

[11] S. Guérin, L.P. Yatsenko, and H.R. Jauslin, Phys. Rev. A **63**, 031403 (2001).

[12] S. Guérin, F. Monti, J.M. Dupont, and H.R. Jauslin, J. Phys. A **30**, 7193 (1997).

[13] S. Guérin, R.G. Unanyan, L.P. Yatsenko, and H.R. Jauslin, Opt. Express **4**, 84 (1999).

[14] L.P. Yatsenko, S. Guérin, and H.R. Jauslin, Phys. Rev. A **65**, 043407 (2002).

[15] H.R. Jauslin, S. Guérin, and S. Thomas, Physica A **279**, 432 (2000).

[16] J.A. Jones, V. Vedral, A. Ekert, and G. Castagnoli, Nature (London) **403**, 869 (2000).

[17] R.G. Unanyan, B.W. Shore, and K. Bergmann, Phys. Rev. A **63**, 043405 (2001).